Supporting Information

Solution-based electrostatic self-assembly routes for obtaining graphene-transition metal dichalcogenide heterostructures

Kenneth Lobo[a], Priyanka R. Sumbe[b], Mahendra A. More[b], Dattatray J. Late[c], and H. S. S. Ramakrishna Matte[a]

[a]*Energy Materials Laboratory, Centre for Nano and Soft Matter Sciences, Arkavathi Campus, Survey No. 7, Shivanapura, Dasanapura Hobli, Bengaluru – 562162, India.*
[b]*Center for Advanced Studies in Material Science and Condensed Matter Physics, Department of Physics, Savitribai Phule Pune University, Pune 411007, India*
[c]*Materials Science and Technology Research Group, Brane Enterprises Private Limited, NSL HUB, Madhapur, Hyderabad, India-500081*

e-mail: krishnamatte@gmail.com, matte@cens.res.in

Experimental procedure

Liquid exfoliation of MoS_2 and graphene using surfactants:

Bulk powders of MoS_2 (Alfa Aeser, 99%) and graphite (SD Fine, 99%) were used as the precursor layered crystals for liquid exfoliation in deionised water along with the surfactants sodium dodecyl sulfate (Sigma Aldrich, 99%) and cetyl tetramethyl ammonium bromide (Sigma Aldrich, 99%), respectively. The bulk powders were taken in a concentration of 30 mg ml^{-1} in 80 mL of water with the surfactant concentration at 10 wt%. Exfoliation was carried out by ultrasonication in a probe sonicator (Vibracell VCX750) at 60% amplitude for 6 hours. Pulsed sonication with a 6 s ON cycle and 2 s OFF cycle were carried out to avoid sample heating, along with water circulation in a cooling jacket around the vessel containing the sonication mixture. Following this, the mixture was subjected to centrifugation in order to separate the exfoliated nanosheets according to size. Centrifugation was carried out for 1 hour at 1000 rpm to remove the bulk unexfoliated powder, and the supernatant was then subjected to cascaded centrifugation at incremental speeds up to 16000 rpm. The sedimented mass containing the size-selected nanosheets were separated carefully after each round of centrifugation by slowly decanting the supernatant which was subjected to further centrifugation, while the sediment was redispersed in deionised water by mild sonication to obtain dispersions of size-selected nanosheets. The dispersions were subjected to two rounds of centrifugation at 16000 rpm, decanting of supernatant, and redispersion with fresh deionized water by sonication, to remove excess surfactant from the nanosheet surfaces/solution.

Similarly, exfoliation by ultrasonication was carried out under similar conditions for $MoSe_2$ (Sigma Aldrich, 99%), WS_2 (Sigma Aldrich, 99%), and WSe_2 (Sigma Aldrich, 99%) with sodium dodecyl sulfate surfactant, followed by ultrasonication at 16000 rpm to obtain the thinnest nanosheets in dispersion.

Heterostructure synthesis:

For synthesizing the heterostructures, graphene and MoS_2 dispersions containing nanosheets of approximately matching lateral dimensions were considered. 2 mL of the MoS_2 dispersions were taken in a 10 mL beaker, under constant stirring using a magnetic bead. The graphene dispersion was then added dropwise while carefully observing the mixture, until a point of flocculation was observed. The formed heterostructures were then characterised by various methods after drying.

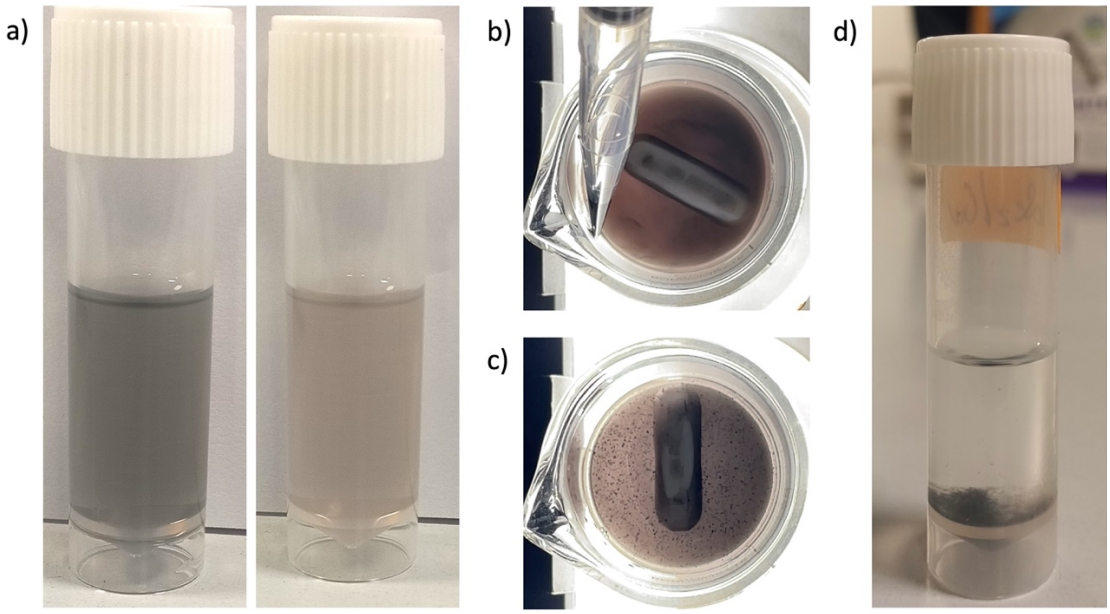

Figure S1. Photographic images showing (a) the starting dispersions of graphene and TMD ($MoSe_2$ in this case), (b) their gradual mixing in a beaker under stirring, (c) resulting in flocculation until (d) complete clarification with the heterostructures settled at the bottom.

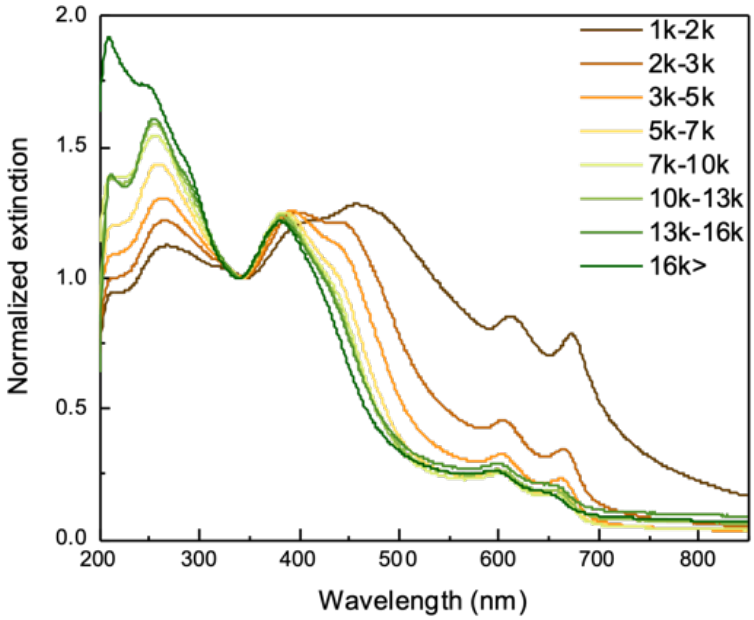

Figure S2. Normalized UV-visible extinction spectra of size-selected MoS_2 nanosheet dispersions.

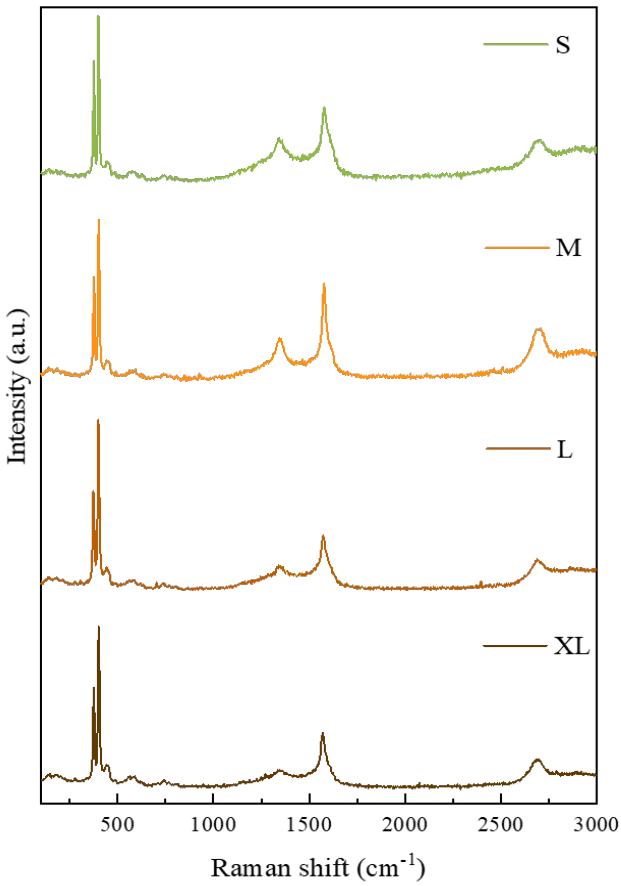

Figure S3. Raman spectra of the flocculation of MoS_2-graphene obtained from four size-selected fractions. The peaks around 400 cm^{-1} correspond to the in-plane (E^1_{2g}) and out-of-plane (A_{1g}) vibrations in MoS_2 layers, while the peaks at 1350 cm^{-1}, 1550 cm^{-1} and 2700 cm^{-1} correspond to the D, G and 2D vibrational modes in graphene, respectively.

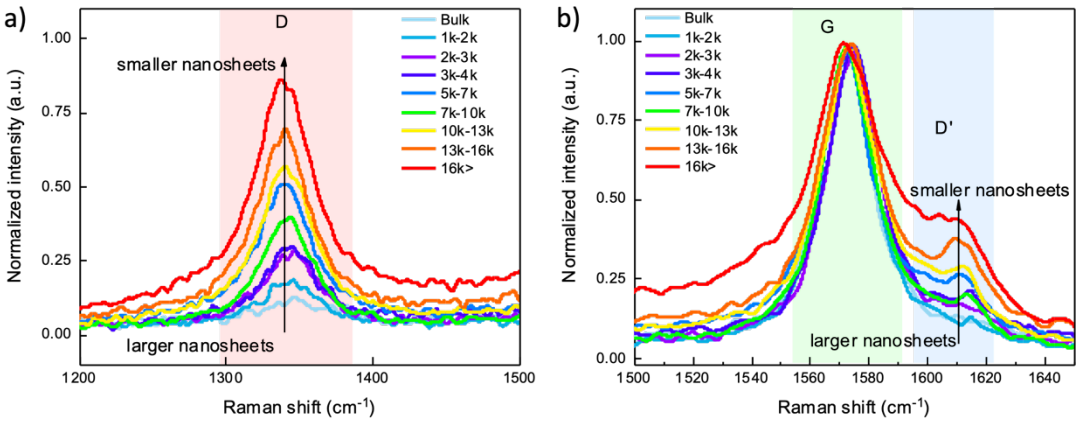

Figure S4. Raman spectra of size-selected graphene nanosheets, normalized to the G peak intensity. Higher D and D' peak intensities were observed for nanosheets obtained at higher speeds.

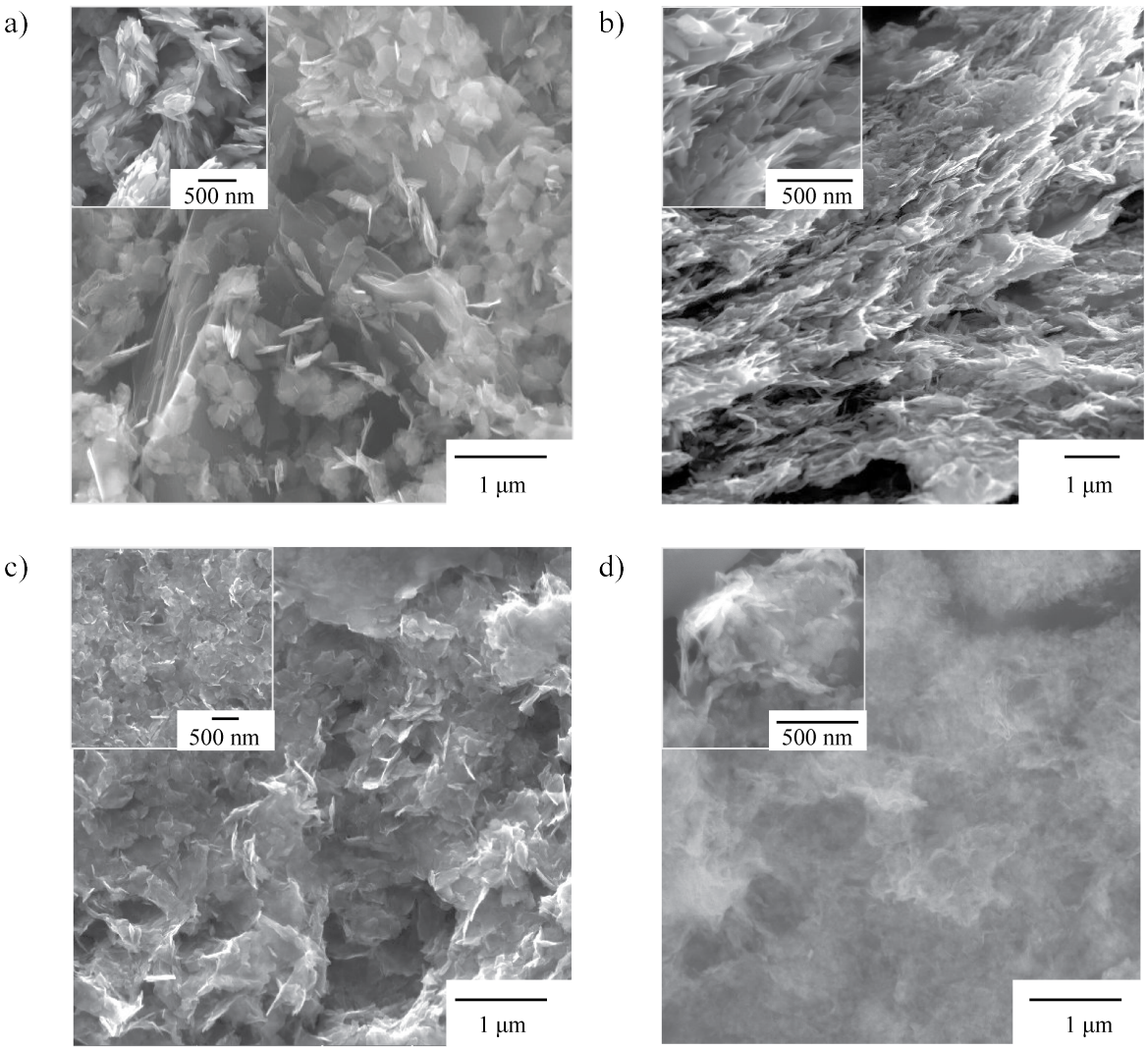

Figure S5. FESEM images for flocculations of MoS_2-graphene prepared with four different nanosheet sizes labelled as (a) XL, (b) L, (c) M, and (d) S. Respective insets show regions at higher magnification.

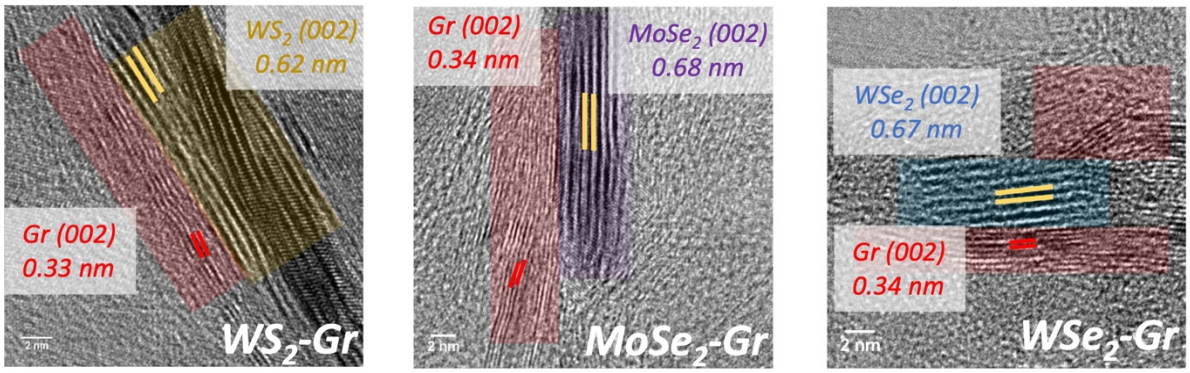

Figure S6. Representative TEM images of heterostructures of graphene with (a) WS_2 (yellow), (b) $MoSe_2$ (purple), and (c) WSe_2 (blue). The regions shaded in red correspond to graphene nanosheets in all three cases.

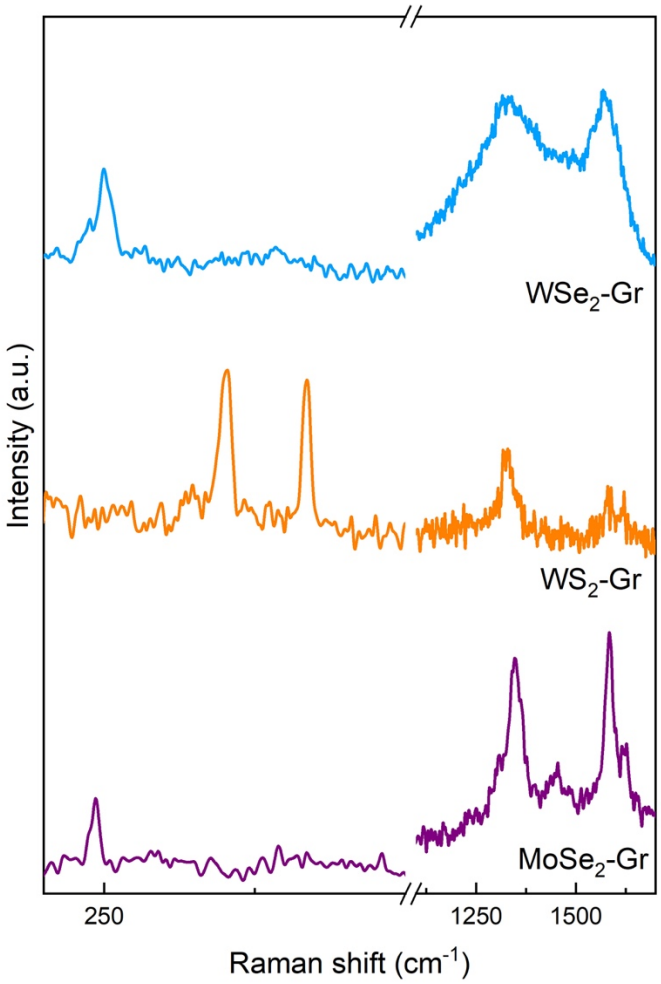

Figure S7. Raman spectra of heterostructures of graphene with $MoSe_2$, WS_2, and WSe_2.

Table S1. Comparison of field emission with 2D materials as emitters.

S. No.	***Field emitters***	***Turn on voltage ($V\ \mu m^{-1}$)***	***Maximum current density ($\mu A\ cm^{-2}$)***	***Reference***
1	Black Phosphorus	5.1 at 1μA/cm²	~312 at 8.7 V/μm	[1]
2	$Ti_3C_2T_x$ MXene	4.7 at 1μA/cm²	~425 at 6.4 V/μm	[2]
3	WS_2	3.5 at 1 μA/cm²	~220 at 6.3 V/μm	[3]
4	WS_2-rGO	2.0 at 1 μA/cm²	~800 at 4.1 V/μm	[3]
5	ReS_2	2.10 at 1 μA/cm²	~850 at 4.0 V/μm	[4]
6	ReS_2-rGO	1.66 at 1 μA/cm²	~1472 at 3.1 V/μm	[4]
7	VS_2	4 at 1 μA/cm²	-	[5]
8	$MoSe_2$	1.9 at 1 μA/cm²	~1509 at 3.9 V/μm	[6]
9	MoS_2 nanosheets	3.5 at 10 μA/cm²	-	[7]
10	MoS_2-rGO	2.6 at 10 μA/cm²	~800 at 3.9 V/μm	[8]
11	**$MoSe_2$**	**2.39 at 1 μA/cm²**	**~32 at 3.65 V/μm**	**This work**
12	**$MoSe_2$-graphene**	**1.91 at 1 μA/cm²**	**~435 at 3.60 V/μm**	**This work**

Field emission with 2D material heterostructures

It was observed that with the same incremental step in applied field, the emission current density initially increases slowly, then rapidly, exhibiting exponential nature over the entire range, as expected by the Fowler-Nordheim (F-N) equation, as stated below,

$$J = a\phi^{-1}E^{2}\exp(-b\phi^{(3/2)}/\beta E)$$

Where, a (≈1.541434 AeVV^{-2}) and b (≈6.830890 eV−3/2 V μm^{-2}) are constants, E is applied electric field, ϕ is work function, and β is the field enhancement factor (also termed as geometric enhancement factor) of the emitter.

The $MoSe_2$–Graphene heterostructures form n-p heterojunctions and its band diagram is schematically depicted below. Since the work function of $MoSe_2$ (φ = 4.65 eV) is greater than that of Graphene (rGO) (φ = 4.5 eV), a Schottky contact is formed at the $MoSe_2$-Graphene interface.[9-11] In order to equalize the chemical potentials in both n- ($MoSe_2$) and p-(Graphene(rGO)) semiconductor semiconductors the band bending occurs, which facilitates flow of electrical charges from RGO to $MoSe_2$ until the two systems attain equilibrium. Thus, the enhanced density of charge carriers in $MoSe_2$ is responsible not only for reducing the turn-on and threshold field values but also enhances the emission current density.

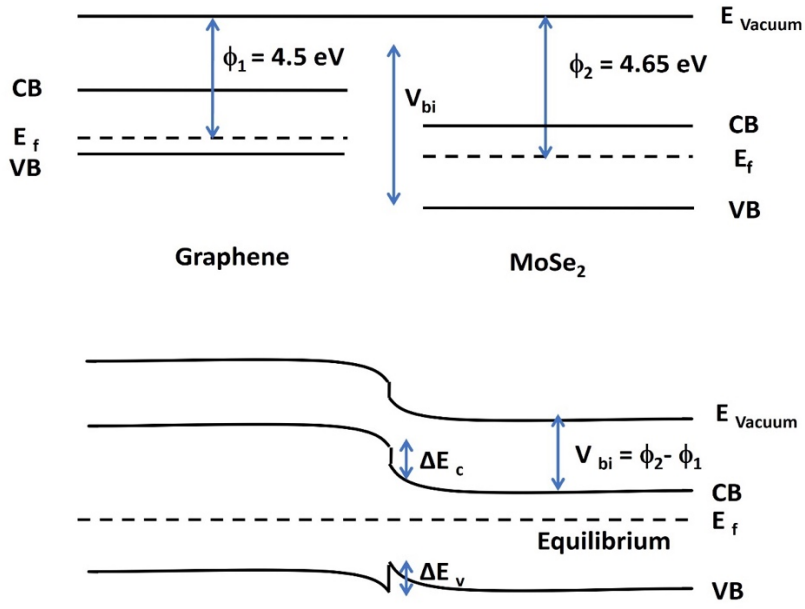

Figure S8. Energy band diagram of $MoSe_2$- Graphene heterostructure. The $MoSe_2$ is n-type semiconductor whereas graphene (rGO) is p-type semiconductor. Here ϕ is work function, CB is conduction band, VB is valence band, E_f is fermi level and V_{bi} is built in voltage.

References

1. S. R. Suryawanshi, M. A. More and D. J. Late, *J. Vac. Sci. Technol. B*, 2016, **34**.
2. N. U. Kiran, A. B. Deore, M. A. More, D. J. Late, C. S. Rout, P. Mane, B. Chakraborty, L. Besra and S. Chatterjee, *ACS Appl. Electron. Mater.*, 2022, **4**, 2656-2666.
3. C. S. Rout, P. D. Joshi, R. V. Kashid, D. S. Joag, M. A. More, A. J. Simbeck, M. Washington, S. K. Nayak and D. J. Late, *Sci. Rep.*, 2013, **3**, 3282.
4. C. D. Mistari and M. A. More, *Nano Exp.*, 2021, **2**, 020018.
5. C. S. Rout, R. Khare, R. V. Kashid, D. S. Joag, M. A. More, N. A. Lanzillo, M. Washington, S. K. Nayak and D. J. Late, *Eur. J. Inorgan. Chem.*, 2014, **2014**, 5331-5336.

6. S. R. Suryawanshi, A. S. Pawbake, M. S. Pawar, S. R. Jadkar, M. A. More and D. J. Late, *Mater. Res. Exp.*, 2016, **3**, 035003.
7. D. J. Late, P. A. Shaikh, R. Khare, R. V. Kashid, M. Chaudhary, M. A. More and S. B. Ogale, *ACS Appl. Mater. Interface.*, 2014, **6**, 15881-15888.
8. S. R. Bansode, K. Harpale, R. T. Khare, P. S. Walke and M. A. More, *Mater. Res. Exp.*, 2016, **3**, 115023.
9. P. Panigrahi, T. Hussain, A. Karton, R. Ahuja, *ACS Sensors*, 2019, 4(10):2646.
10. S. Larentis, B. Fallahazad, E. Tutuc, *Appl. Phys. Lett.*, 2012, 101(22).
11. R. V. Kashid, D. J. Late, S. S. Chou, Y. K. Huang, M. De, D. S. Joag, M. A. More, V. P. Dravid, *Small*, 2013, 9(16):2730.